Investigation into the effectiveness of feed spacer configurations for reverse osmosis membrane modules using Computational Fluid Dynamics

Author links open overlay panel

Omid Kavianipour Gordon D.Ingram Hari B.Vuthaluru

School of Chemical and Petroleum Engineering, Curtin University, GPO Box U1987, Perth, Western Australia 6845, Australia

Received 15 September 2016, Revised 16 December 2016, Accepted 18 December 2016, Available online 20 December 2016.

Journal of Membrane Science
Volume 526, 15 March 2017, Pages 156-171

https://doi.org/10.1016/j.memsci.2016.12.034

Investigation into the effectiveness of feed spacer configurations for Reverse Osmosis membrane modules using Computational Fluid Dynamics

Omid Kavianipour, Gordon D. Ingram, Hari B. Vuthaluru *

School of Chemical and Petroleum Engineering, Curtin University, GPO Box U1987, Perth, Western Australia 6845, Australia

Abstract

Reverse osmosis operations for water treatment are usually energy intensive and responsible for most of the product price. Several studies used flow characteristics to compare different geometries of feed spacers, but these cannot completely explain the effectiveness of feed spacers for promoting mass transfer near membranes. A few recent studies introduced a concept (Spacer Configuration Efficacy, SCE) combining mass transfer and energy consumption, but SCE has been applied only to a limited extent.

The present study uses 3-dimensional steady state Computational Fluid Dynamics with mass transfer to compare four channels with feed spacer configurations (Ladder-type, Triple, Wavy and Submerged) and an empty plain channel using SCE and other performance measures. In contrast to previous studies, a saturated concentration boundary condition is employed at the membrane surface and optimised meshing of the domain is discussed. Power law correlations for SCE and other performance measures developed from the simulation results enable quick evaluation of the spacers.

Results indicated that the assumed saturated solute concentration at the membrane strongly affects the mass transfer coefficient. Based on SCE, the Wavy spacer configuration showed the highest performance for $Re > 120$ among the obstructed geometries considered, while Ladder-type was better for $Re < 120$.

Keywords

Membranes; Computational Fluid Dynamics; Reverse Osmosis; Mass Transfer; Spacer Configuration Efficacy

* Corresponding author.
E-mail address: h.vuthaluru@curtin.edu.au (H.B. Vuthaluru).

1. Introduction

Reverse osmosis (RO) is a common approach to water desalination, mostly used for brackish water in medium to large scale facilities as well as small scale home applications. It relies on an imposed pressure difference to drive the transfer of the desired permeate, water, through a semi-permeable membrane. The membrane is supposed to stop dissolved species and emulsified particles from passing through to the permeate side. Two of the main challenges in RO desalination are reducing energy consumption and the build-up of deposits on the membrane surface leading to frequent outages. Several studies have focussed on different RO membrane variations, helping the desalination industry to have a better understanding of RO modules and to minimize desalination costs.

RO plants require the minimum amount of energy per unit product among the different desalination technologies available today industrially: multi-stage flash, multi-effect distillation, mechanical vapour compression and reverse osmosis [2]. One of the most readily available designs of RO systems is the Spiral Wound Module (SWM), which is made of repeated sandwiches of flat membrane sheets separated by a thin mesh spacer material (Fig. 1). This combination is rolled around a central tube and fitted into a cylindrical body. As the feed flows through the module, a portion passes through the membrane surface, leaving behind a rich brine and producing permeate, which flows into the central collecting tube [3]. SWMs are a compact and cheap option for RO designs offering a high mass transfer area to volume ratio, which leads to high volumetric throughput and moderate energy consumption. In the last few years, several studies have investigated mass transport phenomena or fluid flow to optimize the performance of SWMs. Most of them focused on temperature polarization [4], fluid flow patterns and characteristics [5-9], membrane performance [10] or particle deposition [11]. Limited studies tried to optimize the performance of the modules by changing the spacer configuration to reduce energy consumption and particle deposition while also maximizing fluid mixing and recirculation zone effects. Good spacer configurations should minimize build-up of deposits and concentration polarization by keeping the concentration of the solute in the fluid layer in contact with membrane close to the bulk concentration [5, 6, 12-14]. Table 1 presents a summary of studies conducted on selected SWM spacer configurations from the early 1980s to present.

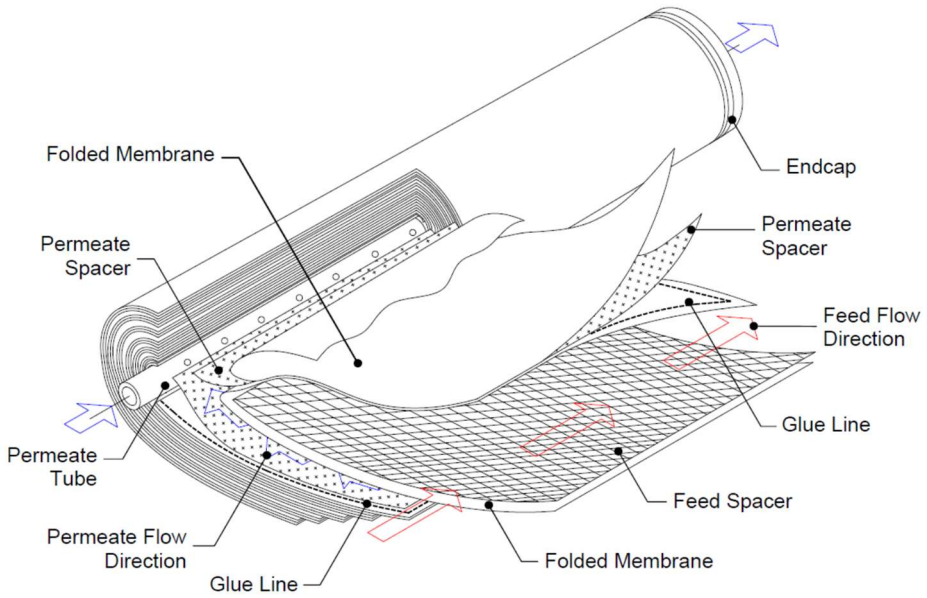

Fig. 1. Configuration of a typical spiral wound module used for reverse osmosis desalination [1].

In general, more mixing in the fluid and more effective recirculating zones will keep mass transfer resistance low and the membrane unblocked. Both effects are characterised by the Sherwood number, Sh. On the other hand, more mixing and flow recirculation means more energy consumption. The final decision on membrane configuration and operating conditions is a trade-off between higher mass transfer rates and longer service intervals between cleaning on one hand, and greater energy costs on the other.

A recent study [13] proposed a dimensionless number that captures both mass transfer, in the form of the Sherwood number, and the energy required for flow, in the form of the Power number, Pn. This dimensionless number, the Spacer Configuration Efficacy (SCE) is defined as Sh/Pn. SCE quantifies mixing quality on the feed side of the membrane for different feed spacer arrangements. Due to its definition, a higher SCE represents a smaller solute concentration difference between the bulk fluid and that near the membrane surface, or a lower pumping energy requirement per unit of permeate. Both mixing quality and recirculating flows will directly influence a unit's energy consumption and increase the maintenance intervals. Saeed, Vuthaluru and Vuthaluru [13] defined the SCE concept and also studied the effect of Re on Pn, Sh, SPC and SCE for Ladder-type spacers and suggested the best geometrical arrangement to use among the different Ladder-type cases studied, but this study needs to be extended to investigate the SCE concept for other spacer configurations.

The main goal of this study is to extend the application of SCE to other spacer geometries and to compare spacer behaviour for varying Reynolds numbers in the laminar regime, up to Re = 200, in terms of both flow characteristics and mass transfer phenomena. Computational fluid dynamics (CFD) will be used to simulate the flow and mass transfer phenomena. Along with commonly reported measures like pressure drop, power consumption and Sherwood number, SCE will also be evaluated from the CFD results, which will allow SCE to be compared against those conventional measures of spacer performance.

Table 1
Summary of previous works focusing on spacer effectiveness in spacer filled RO modules.

Configuration							Investigation type	Reynolds number range	Key channel dimension	Number of cells for CFD studies	Geometrical approximation used for filament near membrane [a]	Boundary condition at membrane	Validation	Major findings	Reference
Zigzag	Cavity	Submerged	Ladder-type	Woven	Obstructed plain channel	Commercial geometries									
×	×						Numerical analysis for Re = 50 – 500; Experimental visualization for Re = 20 – 410	Re_{ch} = 20 – 500	L/H = 5 Centre to centre	Grid size = 67 × 21	Rectangular block	C = 0 (Electrodialysis case)	Original experiments	Visualized flow patterns $Sh = 0.519\ Sc^{0.376}\ Re^{0.475}$ (Zigzag) $Sh = 1.069\ Sc^{0.376}\ Re^{0.294}$ (Cavity)	[15]
						×	Experimental	Re_h = 20 – 2000	Domain size: 2.5 × 40 in	N/A	N/A	N/A	Original experiments	$Sh = 0.065\ Sc^{0.25}\ Re^{0.875}$	[16]
						×	Experimental	Re_h = 150 –1000	Domain size: 35 × 285 mm	N/A	N/A	N/A	Original experiments	They modify the Grober equation for Sh by using a correction factor k_{dc} to increase accuracy: $Sh = 0.664\ k_{dc}\ Sc^{0.33}\ Re^{0.5}\left(\frac{2D_h}{L}\right)^{0.5}$ where $k_{dc} = 1.654\ (d/H)^{-0.039}\ \varepsilon^{0.75}\ (\sin\beta/2)^{0.086}$	[17]
						×	CFD: 3D, steady state	Re_h = 300 – 1800	Domain size: 25 × 35 mm H = 1 – 2 mm	Not mentioned	Filament deformed to octagon	No mass transfer included	Using data provided by [17]	Ten equations for different commercial spacers for the spacer drag coefficient of the form $C_d = A\ /\ (Re)^n$ Velocity distribution reported for some cases.	[18]
×	×	×			×		CFD: 2D, steady state	Re = 120 – 480	Domain size: 2 × 50 mm	15,000	Not mentioned	No mass transfer included	No validation	Flow patterns, shear stress and velocity contours, turbulent kinetic energy diagrams and overall pressure drop.	[19]
×	×	×			×		CFD: 2D, steady state and transient flow	$Re_{ch} \leq 1000$	L/H = 4	Not mentioned	Cylinder cut	No mass transfer included	No validation	Flow patterns, velocity contours and effect of Re on flow disturbance.	[20]
×	×	×					CFD: 3D, steady state	Re_{ch} = 90 – 768	L/d = 1.4 – 75 Centre to centre	22,000	Cylinder cut	No mass transfer included	No validation	Flow patterns, velocity contours, effect of spacer geometry (H/d and L/H) on pressure drop and wall shear stress.	[21]

×	×	×					CFD: 2D, steady state	Re_{ch} = 100 – 400	L/H = 4 & 8 Centre to centre	Not mentioned	Cylinder cut	Constant unmentioned value set for membrane concentration	No validation	Concept of spacer performance ratio introduced as: SPMP = $\frac{\Delta C_{sp}/\Delta C_{slit}}{\Delta P_{sp}/\Delta P_{slit}}$ Zigzag shows the best SPMP.	[22]
			×	×			Experimental; CFD: 3D, steady state Angle of attack: 0, 15, 30 & 45°; filament angle: 60, 90 & 120°	Re = 80 – 550	L/H = 2 – 10 Side to side	Not mentioned	Not mentioned	Not mentioned	Original experiments	SPC, Pn and Sh number for different geometries and different Re.	[23-25]
		×					CFD: 2D, steady state, transient flow	$Re_{ch} \leq 200$	L/H = 3 Centre to centre	5,400	N/A	No mass transfer included	No validation	Velocity contours, shear stress and pressure drop for different Re; flow pattern stable at Re < 60; eddies appear at Re = 78.	[26]
						×	CFD: 3D, steady state	Re_{ch} = 75 – 1500	ϵ = 0.52 – 0.875	150,000	Filament expanded by 7%	No mass transfer included	No validation	Pressure drop, dimensionless pressure drop and shear stress for different geometries and different Re; velocity contours.	[27]
			×				Experimental; CFD: 3D, transient flow	Re_h = 50 – 600 for experiment, Re_h = 67 – 336	L = 3.8, 7.6 & 11.4 mm H = 2 mm Domain size: 30 × 30 mm	500,000	Rectangular block	Not mentioned	Original experiments	Friction factor, flow regime, velocity profile, Reynolds stress tensor, local shear stress, Pn and local Sh for different geometries and Re. S1L0 (L = 3.8 mm, no longitudinal spacer) shows best results.	[28]
		×	×				CFD: 3D, steady state Angle of attack: 30, 45, 60 & 90°	Re_{ch} = 20 – 200	L/H = 2, 3, 4, 6 W/H = 2, 3, 4, 6 Centre to centre	105,000 – 230,000	Cylinder cut	No mass transfer included	± 10% of Li et al. +25% with Koutsou.	Velocity contours and vectors, pressure drop and shear stress for different geometries and Re.	[29]
			×				CFD: 2D/ 3D, steady state Angle of attack: 45 & 90°	$Re_h \leq 1000$	L/H = 4	19 × 10^6	Filament expanded by 20%, rounded edges	Constant concentration at membrane, equal to average concentration result from 2D simulation	Using data provided by [16]	α = 45° shows higher mass transfer. Friction factor, local friction factor, salinity, velocity, Sh, salinity contours with tangential velocity vectors and percentage of energy losses for different Re and geometries.	[30]

			×				Experimental; CFD: 3D	Re_h = 30 – 1000	L/H = 3 Centre to centre	Not mentioned	Not mentioned	No mass transfer included	Original experiments	Model developed agrees with experimental data within 7%. Velocity, shear stress and pressure drop for different lengths with different Re.	[31]
						×	CFD: 3D	Re_h < 200 Fixed inlet flowrate	Different 2, 3 and 4-layer spacers	1,500,000 to 6,700,000	Filament expanded	Constant heat flux at membrane	No validation	Membrane distillation study. Multilayer spacers show higher performance and thinner polarization zones.	[32, 33]
	×						CFD: 2D	Re_{ch} = 150 – 300	L/H = 3, 4	50,000	Cylinder cut	Constant heat flux and unspecified mass fraction at membrane	Using data provided by [16]	Membrane distillation study. Sh-Re results are similar to correlations from [16], but Nu values are underpredicted by 30–50%.	[34]
			×				CFD: 3D, steady state Angle of attack: 0, 45 & 90°	Re_h = 75 – 200	L/H = 2, 3, 4, 6 W/H = 2, 3, 4, 6 Side to side	750,000	Filament deformed by ~15% d	Mass fraction of salt at membrane equal to 1	Using data provided by [23, 29, 35]	Velocity, dimensionless pressure drop, pressure drop, shear stress, mass transfer coefficient, SPC, Pn, Sh and SCE contours with tangential velocity vectors for different Re and geometries. L/H and W/H optimized at 3.6.	[5, 6, 12-14]
			×				Experimental; CFD: 3D Angle of attack: 45°	Re_h = 100 – 1000	L/H = 2.1 Centre to centre	5,300,000	Cylinder cut	No mass transfer included	Original experiments	Steady laminar flow for at Re < 200. Unsteadiness appears at Re ~ 250. Fully turbulent at Re ~ 1000. Appearance of different primary and secondary vortices studied.	[36]
						×	Experimental; CFD: 3D Angle of attack: 45°	Re_h = ~20 – 200	L/H = 4.5 – 5.7	Not mentioned	Not mentioned	No mass transfer included	Original experiments	Shear stress, pressure drop, power number, friction factor and modified friction factor reported for five commercial spacers. X-ray computed tomography used for accurate determination of spacer geometry. Detailed geometries may lead to better local velocity and shear prediction, resulting in better estimation of fouling and concentration polarization.	[37]

a. Different approaches to geometrical approximation of filament near membrane:

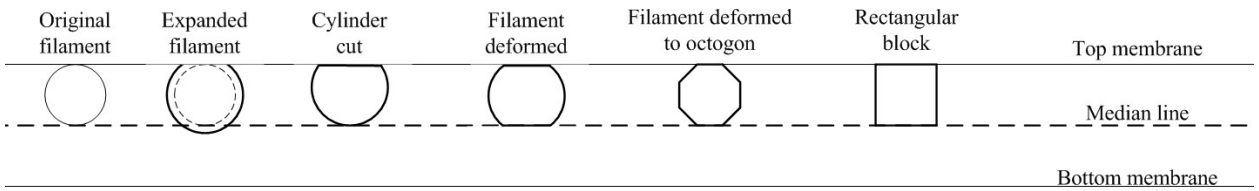
Original filament
Expanded filament
Cylinder cut
Filament deformed
Filament deformed to octogon
Rectangular block
Top membrane
Median line
Bottom membrane

2. Simulation approach

2.1. Geometries studied

In the current work, five spacer geometries have been studied as shown in Fig. 2. Selecting these geometries is based on their widespread use and the availability of data from previous studies, which makes it possible to compare the results. For each geometry, only a representative portion of the fluid flow domain is shown in Fig. 2. The Ladder-type geometry (Fig. 2a) consists of a layer of straight latitudinal filaments positioned on top of a layer of straight longitudinal filaments to form a square pattern. The Triple geometry (Fig. 2b) is a Ladder-type arrangement with a third layer of straight latitudinal filaments added below in the z direction. In the Wavy geometry (Fig. 2c), straight latitudinal filaments are located alternatively adjacent to the top and bottom membranes with sinusoidal longitudinal filaments weaving between them. The Submerged geometry (Fig. 2d) has latitudinal filaments only, positioned midway between the top and bottom membranes. Finally, the Plain geometry (Fig. 2e) represents an unobstructed channel between two parallel membrane surfaces; that is, no spacer filaments are present in this geometry. All filaments are assumed to have a circular cross-section which, while not exactly true for commercial spacers, is a reasonable assumption [37]. Biplanar feed spacer geometries are most the most widely used type for RO modules [1], which

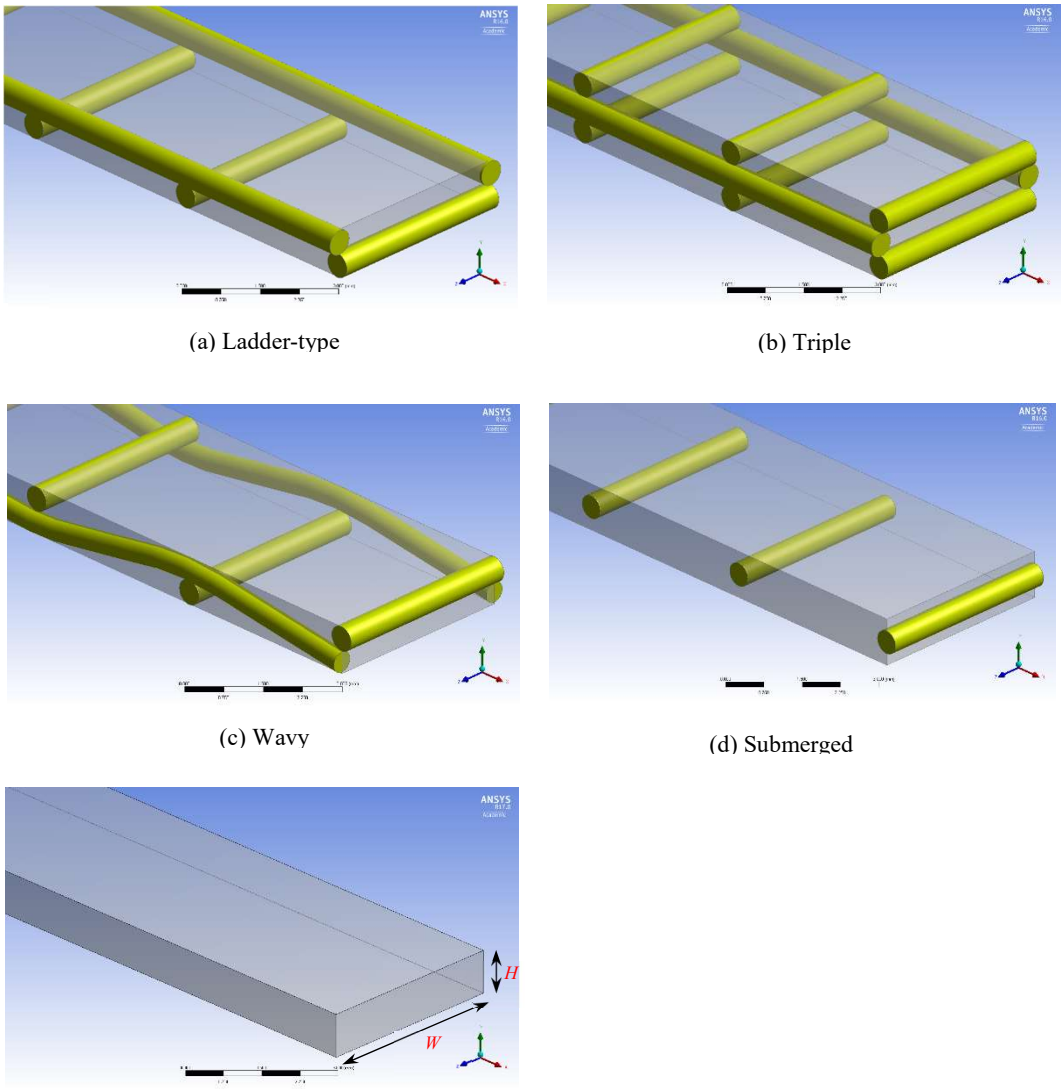

(a) Ladder-type (b) Triple

(c) Wavy (d) Submerged

(e) Plain

Fig. 2. Schematic diagram of feed spacer geometries considered in the present study.

means both Plain and Triple are not common choices for membrane systems, but they are included for comparison purposes with the other more conventional configurations.

2.2. Parameters considered for simulation

Hydraulic diameter (D_h)

The hydraulic diameter, D_h, is defined as

$$D_h = \frac{4 \times volume\ occupied\ by\ fluid}{surface\ area\ of\ wetted\ walls} \quad (1)$$

For flow in membrane channels with spacer filaments, this becomes [16]

$$D_h = \frac{4 \times (channel\ volume - filament\ volume)}{membrane\ surface\ area + filament\ surface\ area} \quad (2)$$

Due to necessary approximations in the filament geometry, which will be discussed in Section 2.5, the volumes and surface areas in this study were carefully extracted from the CFD software used.

Effective velocity (u_{eff})

The effective velocity, u_{eff}, is defined [16] as the volumetric flowrate, $\dot{V}$, divided by the effective area for flow:

$$u_{eff} = \frac{\dot{V}}{A_{eff}} \quad (3)$$

The effective area, A_{eff}, is equal to the cross-sectional area of the channel in the flow direction, assuming no filaments are present, multiplied by the porosity of the channel system:

$$A_{eff} = WH\epsilon \quad (4)$$

where W is the channel width, H is the channel height and the porosity is

$$\epsilon = 1 - \frac{filament\ \ volume}{unobstructed\ channel\ volume}$$

The effective velocity characterizes the 'sweeping velocity' or 'bulk average velocity' of fluid in the channel.

Hydraulic Reynolds number (Re)

In the present study, the hydraulic Reynolds number has been used to represent different flowrates through the membrane system. This definition was also used in previous studies [5, 16, 30]. All cases considered in the present study were in the laminar flow regime, with Re varying between 50 and 200. The notation Re is used throughout this paper to mean the hydraulic Reynolds number:

$$\mathrm{Re} = \frac{\rho u_{eff} D_h}{\mu} \quad (5)$$

It should be noted that other definitions of the Reynolds number also appear in the literature. They differ in the velocity and characteristic length used. For example, the filament diameter and average velocity gives the cylinder Reynolds number ($\mathrm{Re_{cyl}}$) while the channel height and average velocity

leads to the channel Reynolds number (Re_{ch}). The different definitions and their characteristics have been discussed elsewhere [5].

Specific Power Consumption (SPC)

SPC represents the mechanical energy required to overcome the fluid's pressure drop per unit length of the domain [39]. Storck and Hutin [40] define SPC as

$$SPC = u_{eff}\frac{\Delta P}{L} \tag{6}$$

where $\Delta P/L$ is the pressure drop per unit length in the main flow direction. A slight manipulation shows that $SPC = (A_{eff}u_{eff}\,\Delta P)/(A_{eff}L)$; that is, SPC is the power consumed per unit volume of fluid. Several authors have studied SPC and its relation with different geometries and Reynolds numbers [6, 7, 13, 15, 24-26].

Power number (Pn)

The Power number, Pn, is another term suggested in the literature to represent power consumption in a membrane module. Li, Meindersma, de Haan and Reith [24] introduced Pn after a dimensional analysis to represent the amount of power required to drive the RO operation; the use of Pn was continued in Li and Tung [31], Saeed [5], and Haaksman, Siddiqui, Schellenberg, Kidwell, Vrouwenvelder and Picioreanu [37].

The Power number is defined as

$$\mathrm{Pn} = \mathrm{SPC}\left(\frac{\rho^2 H^4}{\mu^3}\right) = \frac{\Delta P}{L}\left(\frac{u_{eff}\rho^2 H^4}{\mu^3}\right) \tag{7}$$

It can be rearranged as $\mathrm{Pn} = \left(\frac{\Delta P}{\rho {u_{eff}}^2}\right)\left(\frac{u_{eff}\,\rho\,D_h}{\mu}\right)^3\left(\frac{H}{L}\right)\left(\frac{H}{D_h}\right)^3 = \mathrm{EuRe}^3\left(\frac{H}{L}\right)\left(\frac{H}{D_h}\right)^3$, where Eu is the Euler number. Considering this rearrangement, Pn can be interpreted as shown below:

(pressure forces / inertial forces) × (inertial forces / viscous forces)^3 × (geometrical ratios).

The Power number is also considered to be a modified friction factor [38].

Dimensionless pressure drop (ΔP^*)

In 1987, Schock and Miquel [16] introduced a dimensionless friction factor to interpret their experiments, but recently Shakaib, Hasani and Mahmood [29] and Koutsou, Yiantsios and Karabelas [35] used a new dimensionless pressure drop, ΔP^*, defined as

$$\Delta P^* = \frac{\Delta P}{L}\left(\frac{{D_h}^3}{\mathrm{Re}_{\mathrm{cyl}}^2 \rho {u_{eff}}^2}\right) \tag{8}$$

Sherwood number (Sh)

The Sherwood number is defined as

$$\mathrm{Sh} = \frac{kD_h}{\mathcal{D}} \tag{9}$$

where k is the average mass transfer coefficient, the hydraulic diameter is used as the characteristic length and $\mathcal{D}$ is the molecular diffusivity of the solute (NaCl) in water.

In the present study, k is calculated from the difference of salt mass flowrate in the inlet and outlet flows, the arithmetic mean salt concentration driving force and the membrane surface area:

$$k = \frac{Outlet\ salt\ mass\ flow\ rate\ (\mathrm{kg/s}) - Inlet\ salt\ mass\ flow\ rate\ (\mathrm{kg/s})}{(membrane\ area\ (\mathrm{m^2})) \times (mean\ concentration\ difference\ between\ membrane\ and\ bulk\ fluid\ (\mathrm{kg/m^3}))} \quad (10)$$

The result is an average Sh that accounts for mass transfer through both top and bottom membranes. The value of k calculated using a logarithmic mean driving force was negligibly different from that calculated using the arithmetic mean over the range of conditions explored in this study.

Spacer Configuration Efficacy (SCE)

Saeed [5] recently defined a new dimensionless number, SCE, for use in membrane spacer investigations that combines both mass transfer and pressure drop phenomena:

$$\mathrm{SCE} = \frac{\mathrm{Sh}}{\mathrm{Pn}} \quad (11)$$

SCE aims to represent the amount of mass transfer for a given amount of consumed energy. Higher SCE is caused by higher mass transfer or lower energy requirements, which indicates a more effective spacer. This approach was used in our earlier efforts [5, 13].

2.3. Governing equations, modelling software and solution options

The Navier-Stokes equations were used to describe conservation and transport processes as shown below. The fluid was assumed to be Newtonian, while the flow was assumed to be steady state and laminar.

$$\frac{\partial u}{\partial x} + \frac{\partial v}{\partial y} + \frac{\partial w}{\partial z} = 0 \quad (12)$$

$$u\frac{\partial u}{\partial x} + v\frac{\partial u}{\partial y} + w\frac{\partial u}{\partial z} = -\frac{1}{\rho}\frac{\partial P}{\partial x} + \frac{\mu}{\rho}\left[\frac{\partial^2 u}{\partial x^2} + \frac{\partial^2 u}{\partial y^2} + \frac{\partial^2 u}{\partial z^2}\right] \quad (13)$$

$$u\frac{\partial v}{\partial x} + v\frac{\partial v}{\partial y} + w\frac{\partial v}{\partial z} = -\frac{1}{\rho}\frac{\partial P}{\partial y} + \frac{\mu}{\rho}\left[\frac{\partial^2 v}{\partial x^2} + \frac{\partial^2 v}{\partial y^2} + \frac{\partial^2 v}{\partial z^2}\right] \quad (14)$$

$$u\frac{\partial w}{\partial x} + v\frac{\partial w}{\partial y} + w\frac{\partial w}{\partial z} = -\frac{1}{\rho}\frac{\partial P}{\partial z} + \frac{\mu}{\rho}\left[\frac{\partial^2 w}{\partial x^2} + \frac{\partial^2 w}{\partial y^2} + \frac{\partial^2 w}{\partial z^2}\right] \quad (15)$$

$$u\frac{\partial C}{\partial x} + v\frac{\partial C}{\partial y} + w\frac{\partial C}{\partial z} = \mathcal{D}\left[\frac{\partial^2 C}{\partial x^2} + \frac{\partial^2 C}{\partial y^2} + \frac{\partial^2 C}{\partial z^2}\right] \quad (16)$$

Inlet boundary conditions:

$$C = C_i; \qquad u = \frac{\dot{m}}{\rho A_i}; \qquad v = w = 0$$

Membrane boundary conditions:

$C = C_m;$ $\quad u = v = w = 0$

Filament boundary conditions:

$\frac{\partial C}{\partial n} = 0;$ $\quad u = v = w = 0$

Symmetry face boundary conditions:

$\frac{\partial C}{\partial z} = 0;$ $\quad \frac{\partial u}{\partial z} = \frac{\partial v}{\partial z} = \frac{\partial w}{\partial z} = 0$

Outlet boundary condition:

$P = P_0$

In the present study, different ANSYS 15.0 and 16.0 modules were used to simulate the flow through the membrane feed channels: ANSYS Geometry, ANSYS Meshing, ANSYS Fluent and ANSYS Workbench. The models were run on a PC equipped with an E5-1650v2 Intel Xeon CPU with 6 HT cores 3.5 GHz, 1×NVIDIA Quadro K2000 and 80 GB of ECC Registered DDR3 memory running at 1866 MHz. All parameter values used in this study are given in Sections 2.4–2.6.

For the Fluent solver, the Coupled Scheme was chosen as it offers steady convergence and a minimum of fluctuation through the iterations. For spatial discretization, the Green-Gauss Node Base method was used for Gradient, Second Order for pressure and Third Order MUSCL for momentum and salinity calculations. The maximum accepted error was set to 10^{-5}.

2.4. Domain

The unit cell is the rectilinear region on the feed side of a membrane system bounded above and below by the membrane surfaces and aligned with the filament centrelines such that it contains fluid and portions of adjacent spacer filaments that could be repeated to reconstruct the entire feed-side geometry. Fig. 3 shows a typical unit cell. In the present study, the domain of the simulated fluid channel was 9 unit cells long and 1 unit cell wide (Fig. 4). Flow enters the domain through the inlet face in the *x* direction, continues through the channel and leaves the domain at the outlet face. The recent literature reveals that the fluid flow will be fully developed after 3 or 4 unit cells [5]. If it is assumed conservatively that outlet affects the flow similarly then, in the present study, the fifth unit cell will be most representative of fully developed conditions. It should be noted that other studies assume that one unit cell only is affected by the outlet, but they do so without any proof or justification [5].

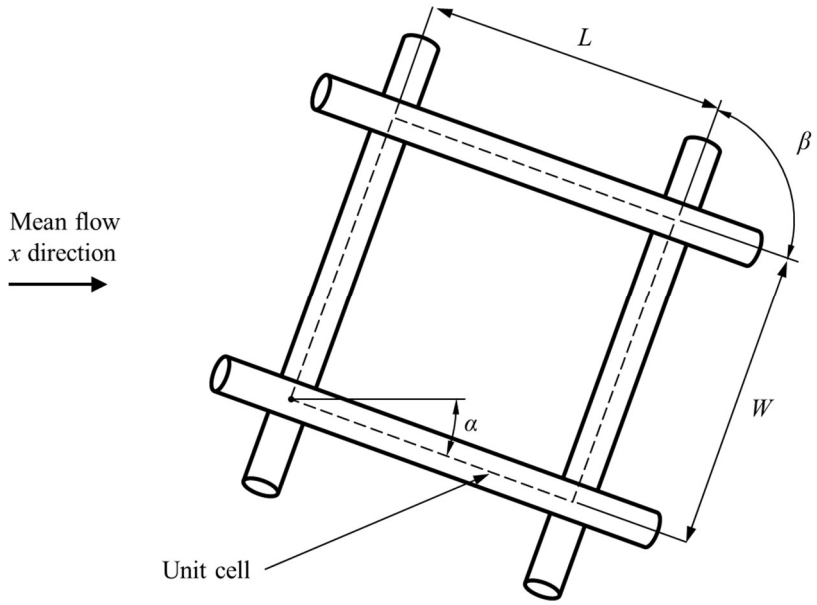

Fig. 3. Plan view of a unit cell for a typical spacer geometry showing the flow angle of attack (α), spacer geometry angle (β), spacing between longitudinal filaments or channel width (W), and spacing between latitudinal filaments or channel length (L).

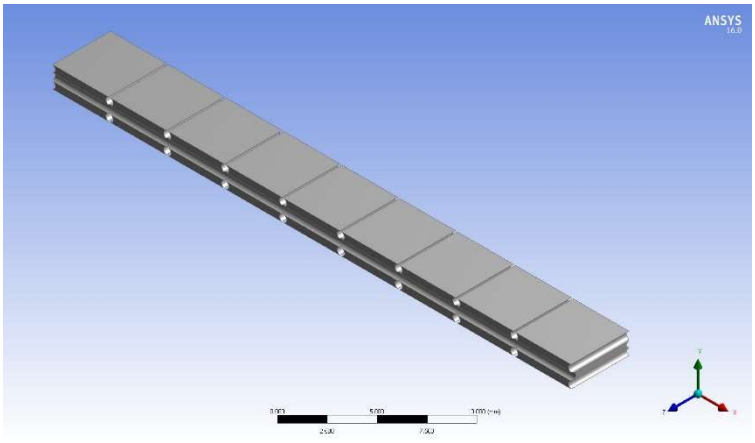

Fig. 4. Example of the simulation domain for the Triple spacer geometry: 9 unit cells long by 1 unit cell wide.

2.5. Mesh generation

The interface between the cylindrical filaments and the flat membrane is impossible to mesh and model perfectly. No clear explanations or discussions are found in the literature about this specific meshing problem and its possible solutions, but from published figures it can be deduced that two approaches have been taken: (i) using a deformed filament [5, 12, 13] wherein the circular filament is approximated by a polygon or the major segment of a circle, and (ii) slightly increasing the filament diameter allowing the filament and membrane to overlap partially [21, 41]. In the present study, both methods have been used. Filament extension was used for the Zigzag and Triple geometries and the deformed filament method was used for the Wavy geometry. Preliminary investigations revealed that

a 1% extension or cutting based on the filament diameter is the minimum amount of deformation that results in acceptable mesh quality and solution convergence. The available processing power (as detailed in Section 2.3) limits the meshing quality. In other words, using a larger amount of deformation results in more relaxed meshing and a lower number of cells, but it decreases simulation accuracy.

Hexahedral meshes have been used in many previous studies [4-6, 12, 13, 18, 20-22, 27-29, 42]. However, in the current study, tetrahedral meshes showed lower skewness values and led to quicker and more stable convergence than hexahedral meshes. Hence, tetrahedral cells were used for meshing all models in this work.

In the present study, mesh independence was investigated for the Ladder-type geometry and then the same sizing rules were used for the Submerged and Plain geometries. More detailed meshing was needed for the Wavy and Triple geometries to achieve convergence. As it is important to make the mesh finer close to the filaments and membrane while keeping the total number of elements as low as possible, two local meshing rules were defined in those regions.

To ensure mesh independence, the number of cells was increased until the change in key results, such as the total pressure drop and outlet salt mass flowrate, became less than 2%. Table 2 reports the final mesh size settings, as defined for ANSYS Meshing. The curvature angle and growth rate shown in the table are, respectively, a measure of the maximum allowed deviation from a flat plane for curved mesh faces and the maximum allowed ratio of the cell sizes of neighbouring cells. To the best of our knowledge, no other studies have reported this detailed meshing information; thus no comparison is possible for the meshing part of this study.

Table 2
ANSYS Meshing mesh size settings used in this study.

Parameter	Default value	Body	Membrane	Filament
Curvature normal angle (°)	18	18	18	6
Minimum size (m)	Based on geometry	1×10^{-7}	1×10^{-7}	1×10^{-7}
Growth rate	1.15	1.15	1.03	1.08

Fig. 5 is an example of meshing for the Ladder-type geometry, which shows one of the corners of the domain, including both longitudinal and latitudinal filaments.

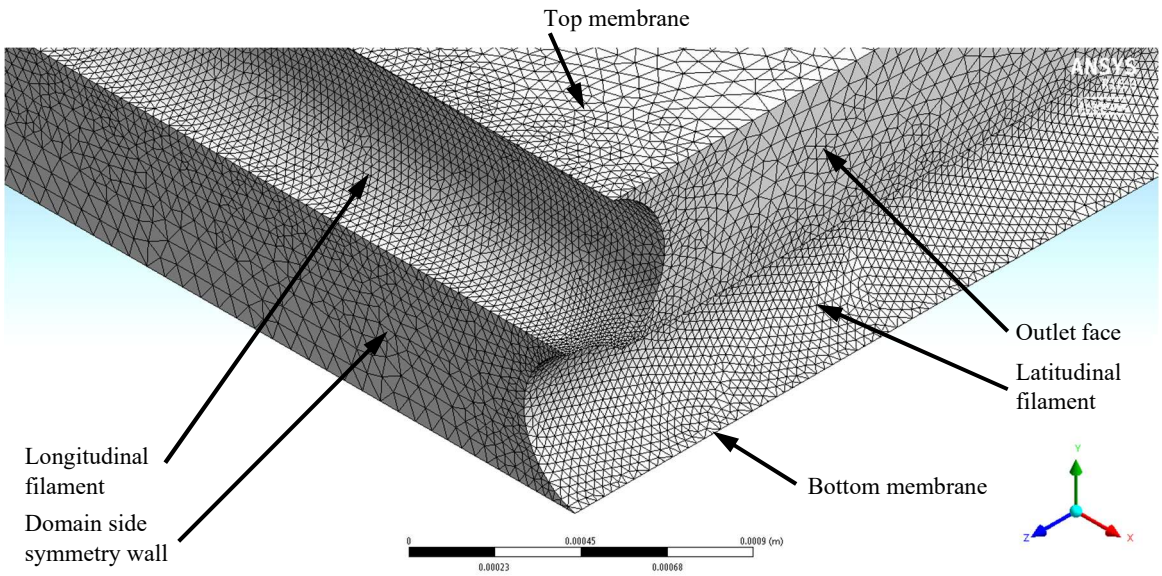

Fig. 5. Typical example of meshing for the Ladder-type spacer geometry.

2.6. Simulation parameters

In the present study, the filament diameter is fixed at d = 0.5 mm. The channel height, H, is set to $2d$ for all geometries, except for the Triple where it is $3d$, and the channel width is $W = 4.1 \times 2d$ in all cases (Fig. 3), which was suggested as the most efficient size in [14]. In all cases, the cells are square, meaning the longitudinal and latitudinal filament spacing is the same, $L = W$, and the geometry angle $\beta = 90°$. The domain is 9 unit cells long, as discussed in Section 2.4.

The physical properties of the fluid are constant and assumed to be those of pure water, except for density, which was calculated as a weighted average based on the concentration. Capobianchi, Irvine, Tutu and Greene [43] showed that NaCl diffusivity in water can be assumed to be constant, regardless of solute concentration.

The feed fluid enters the domain in the x direction, normal to the vertical inlet face. It consists of saline water with a concentration C_i = 5% w/w NaCl. The inlet mass flowrate was varied to provide the required hydraulic Reynolds numbers.

The outlet face at the far end of the channel is parallel to the inlet face and is defined as a pressure outlet. All the fluid entering the domain flows out through this face.

Both membrane planes and all filament surfaces were defined as no-slip, stationary walls. The membranes were assumed to be non-porous and impermeable, and with a fixed concentration boundary condition of C_m = 35% w/w NaCl to represent saturated conditions [44] at the membrane surface. Various recent studies [5, 6, 12, 13] have used a similar fixed concentration boundary condition at the membrane surface, but they assumed 100% w/w NaCl concentration, which possibly represents the presence of a worst-case fouling layer. As it is preferable to keep the membrane free from fouling in practice, the saturated value was used for the concentration boundary condition at the membrane surface in the current study.

In all the geometries considered in this study, the spacer was aligned with the mean flow direction (corresponding to $\alpha = 0°$ in Fig. 3). Consequently, symmetry wall boundary conditions were used for

the side boundaries of the channel not occupied by filament (Fig. 5). All filaments were defined as solid surfaces, allowing no water or salt to pass through.

The parameter values used in the simulations are summarised in Table 3.

Table 3
Modelling input parameters used in the present study.

Parameter	Value
Geometrical parameters	
d	0.0005 m
H	$\begin{cases} 0.0015 \text{ m (Triple geometry)} \\ 0.001 \text{ m (other geometries)} \end{cases}$
$W = L$	0.0041 m
α	0°
β	90°
Physical properties	
ρ	998.2 kg/m^3 [45]
μ	0.001 Pa.s [46]
$\mathcal{D}$	1.52×10^{-9} m^2/s [43]
Operating conditions	
Re	50, 100, 150, 200
C_i	5% w/w NaCl
C_m	35% w/w NaCl

3. Results and Discussion

Simulation runs covering 20 different cases were performed. The calculated performance measures, such as SPC, Pn and ΔP^* are based on the weighted average values extracted from ANSYS Fluent.

3.1. Effect of Reynolds number

The main goal of this study is to investigate the effectiveness of different feed spacers for different production rates. Previous studies occasionally used the mass flowrate or velocity to identify different cases, but due to differences in channel height and configuration, most studies choose the Reynolds number to facilitate the comparison of results.

Table 4 presents power law equations that approximate the CFD results. These equations are helpful for both interpreting and summarising the results. The parameters of the power law equations were obtained using Matlab that maximized the coefficient of determination, R^2. All equations have R^2 of 0.995 or higher, except for the Sh-Re and Sh-Pn equations for the Ladder-type and Triple geometries, where it was as low as 0.97. In Figures 6–11, the symbols depict the CFD results, while the lines show the predictions of the power law correlations reported in Table 4.

It should be noted that each correlation was based on the four values of Re considered in the current work. High values of R^2 for pressure drop, SPC, Pn and SCE represent better predictability for these parameters.

Table 4
Geometrical parameters of the spacers and correlations for key variables derived from the CFD simulations.

Configuration	Ladder-type	Triple	Wavy	Submerged	Plain	
D_h (mm)	1.31	1.72	1.29	1.60	2.00	
A_{eff} (mm^2)	3.71	5.56	3.71	3.90	4.10	
ϵ	0.904	0.904	0.904	0.952	1.00	
						Min. R^2
$\Delta P/L$ (Pa/m)	4.16 Re $^{1.49}$	2.85 Re $^{1.55}$	6.17 Re $^{1.37}$	9.97 Re $^{1.29}$	5.58 Re $^{1.06}$	0.9994
SPC (W/m^3)×10^3	2.69 Re $^{2.52}$	1.42 Re $^{2.45}$	4.20 Re $^{2.40}$	5.32 Re $^{2.32}$	2.66 Re $^{2.07}$	0.9999
Pn	4.37 Re $^{2.42}$	11.6 Re $^{2.48}$	5.86 Re $^{2.33}$	7.92 Re $^{2.24}$	2.92 Re $^{2.05}$	0.9999
ΔP^*	3.08 Re $^{-0.596}$	4.78 Re $^{-0.533}$	3.99 Re $^{-0.680}$	6.86 Re $^{-0.774}$	2.97 Re $^{-0.955}$	0.9946
Sh	10.1 Re $^{0.341}$	8.43 Re $^{0.425}$	3.62 Re $^{0.549}$	5.85 Re $^{0.382}$	8.94 Re $^{0.257}$	0.9743
	8.96 Pn $^{0.140}$	5.67 Pn $^{0.169}$	2.44 Pn $^{0.234}$	4.17 Pn $^{0.169}$	7.83 Pn $^{0.125}$	0.9690
SCE	1.48 Re $^{-1.96}$	0.419 Re $^{-1.93}$	0.530 Re $^{-1.75}$	0.640 Re $^{-1.83}$	2.89 Re $^{-1.78}$	0.9996

3.1.1. Pressure drop

Fig. 6 shows for all geometries that the pressure drop per unit length increases with Reynolds number. As expected, the Plain channel has by far the lowest pressure drop, approximately 20% that of the other types, because there are no filaments to obstruct the fluid flow. In addition, the pressure drop for the Plain channel increases essentially linearly with Re (as can be seen in Table 4), while for the other geometries the dependence is proportional to $Re^{1.3–1.5}$. A closer examination of the geometries with filaments in Fig. 6 and Table 4 shows the Triple and Wavy geometries have the lowest pressure drop at low Re, and Triple increases most quickly with Re ($\propto Re^{1.55}$) while Wavy increases more slowly ($\propto Re^{1.37}$). This results in the Wavy geometry having the lowest pressure drop of the spacer types considered for Re > 80. Shakaib, Hasani and Mahmood [29] report a pressure drop of 3500 Pa/m for a Ladder-type spacer with $W = L = 4H$ at Re = 100, which differs by about 10% from the results reported in Fig. 6, where $W = L = 4.1H$.

In terms of pressure drop, the Wavy configuration seems to be the best choice among the configurations tested. It is thought that this behaviour is a result of the sinusoidal longitudinal filaments (Fig. 2c) helping guide the flow around the latitudinal filaments with less resistance and smoothing the eddy flows downstream of the latitudinal filaments, which are responsible for part of the energy loss.

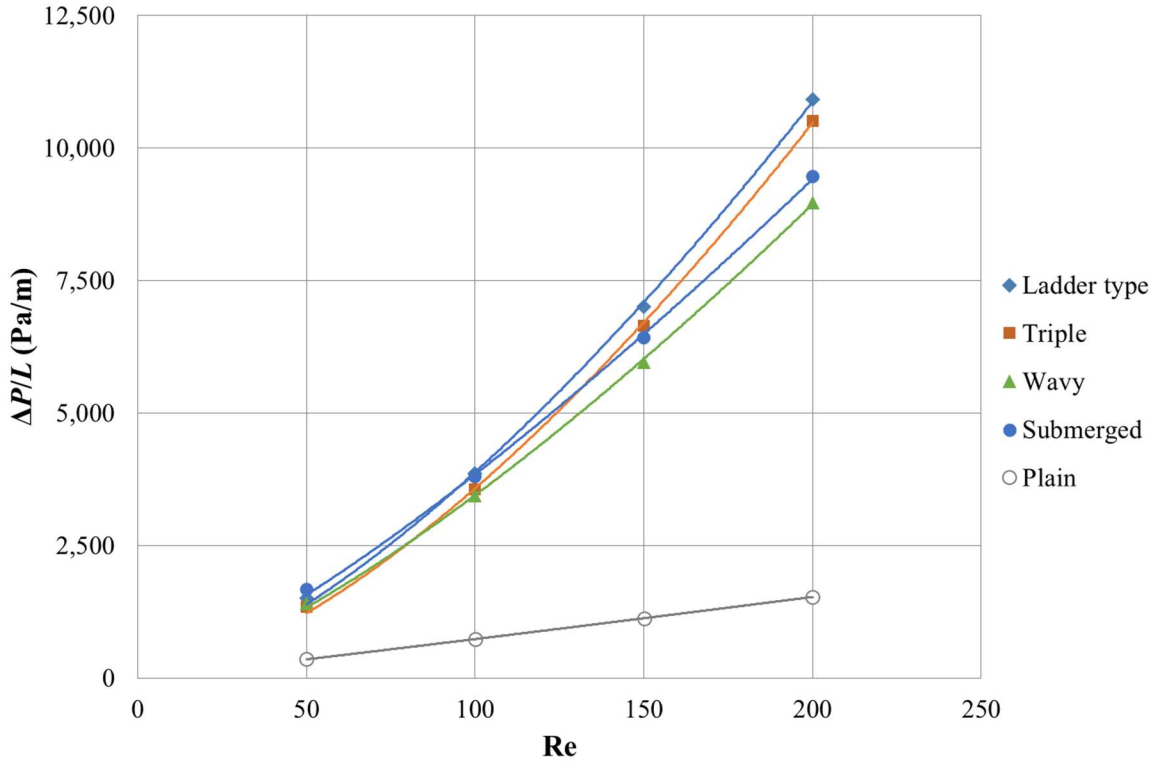

Fig. 6. Predicted pressure drop per unit length as a function of Re for the five spacer geometries.

3.1.2. Power consumption

Fig. 7 indicates that SPC increases rapidly as the flowrate increases. The Plain channel has the lowest SPC, which, as before, is a result of the lack of obstructions in the flow domain. Of the other geometries, the Ladder-type has the highest SPC while Triple and Submerged have the lowest. The highest rate of increase of SPC is for the Ladder-type geometry, which has SPC $\propto$ $Re^{2.5}$, while the lowest is for Submerged, where SPC $\propto$ $Re^{2.3}$ (Table 4).

Since Pn is proportional to SPC×H^4 (Eq. 7) and the fluid properties are constant, the trends of Pn with Re mirror those for SPC for the spacers with the same channel height, H (Fig. 8). The exception is the Triple geometry, which has $H = 3d$ compared to $H = 2d$ for the other geometries, resulting in Pn that is around 4 times higher than for the other geometries with filaments. It should be noted that, excluding the Plain geometry, the exponents of Re in the power law correlations for Pn reported in Table 4, and shown in Fig. 8, (2.24–2.48) are in good agreement with the range of Re exponents (2.25–2.83) reported in [37] for a selection of commercial spacers.

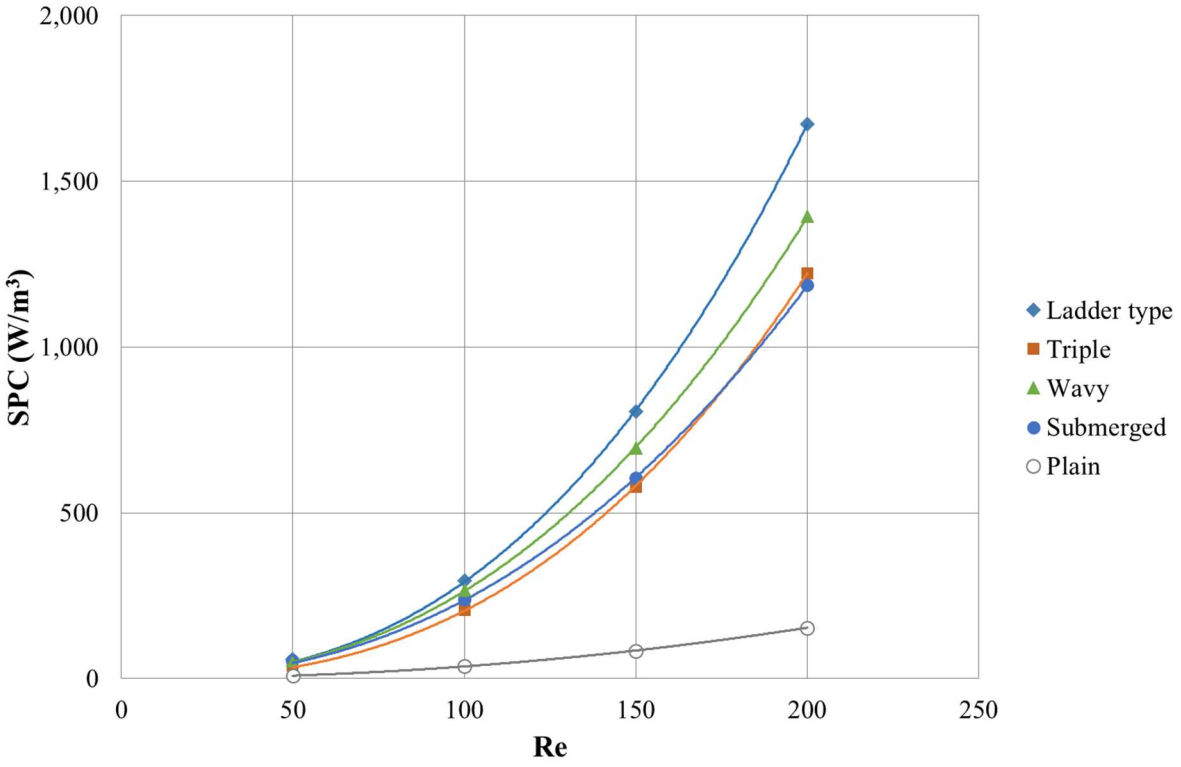

Fig. 7. Predicted Specific Power Consumption as a function of Re for the five spacer geometries.

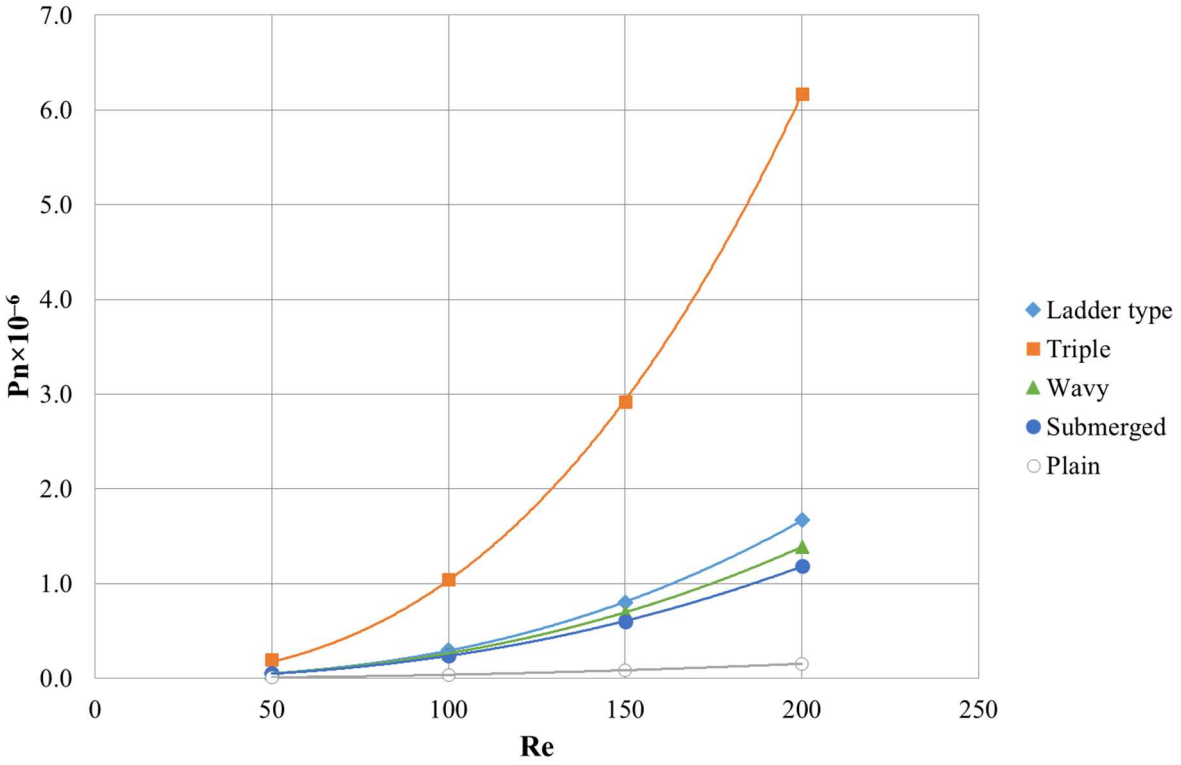

Fig. 8. Predicted Power number as a function of Re for the five spacer geometries.

3.1.3 Mass transfer

Fig. 9 shows the relationship between Sh and Re. In all cases, the Sherwood number increases with increasing Reynolds number. The Triple geometry has the highest Sh while the Plain channel has the lowest Sh of all those studied.

Sherwood number is plotted against Power number in Fig. 10 in an attempt to find the spacer with the best trade-off between production capacity and energy consumption. In previous work, the Sh-Pn relationship has been studied using simulation and experimental data by [23, 24] for a Ladder-type geometry with $L = 4d$, $\alpha = 0°$ and $\beta = 90°$. Also the overall trend and form of equations provided by other researchers [15, 17, 38] is in accordance with our results in Figs 9 and 10.

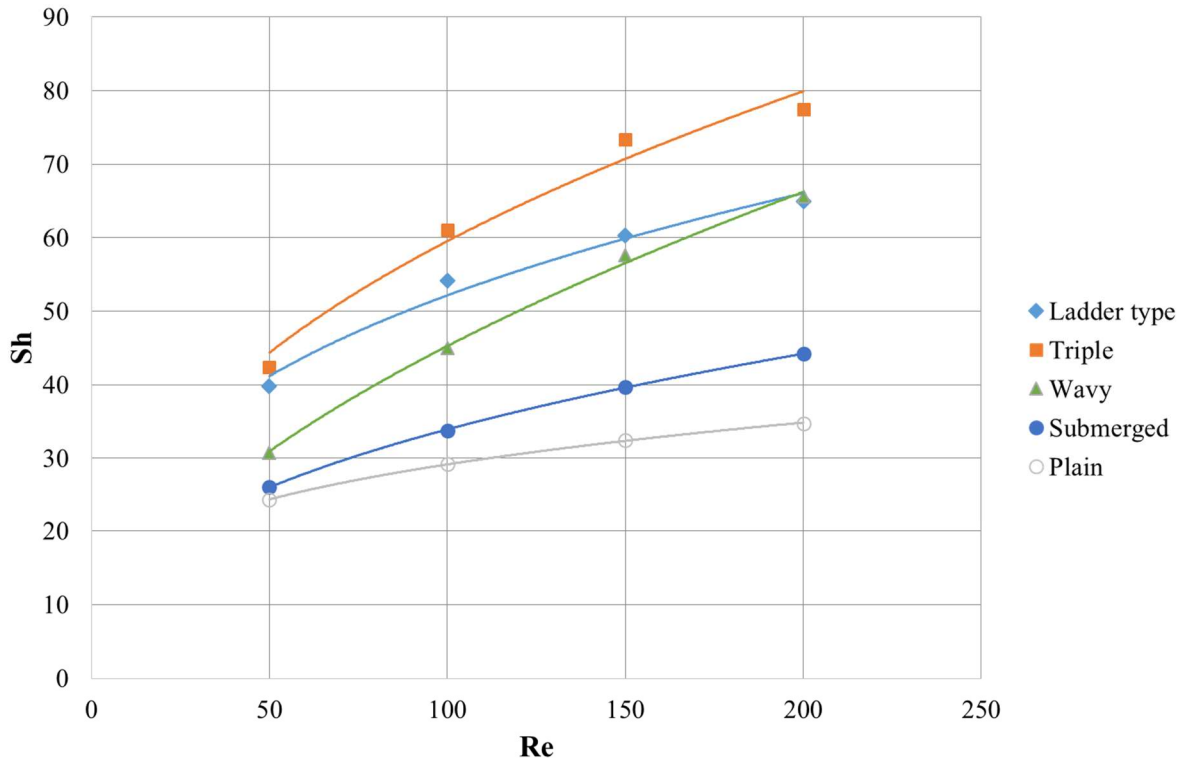

Fig. 9. Predicted Sherwood number as a function of Re for the five spacer geometries.

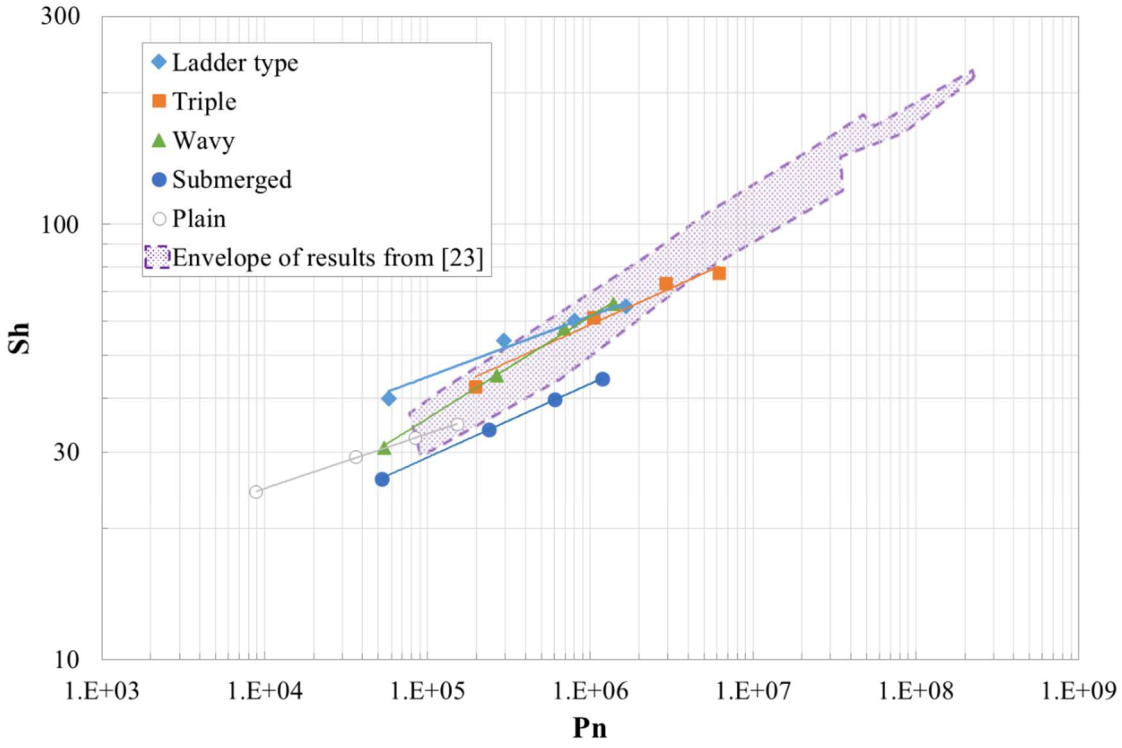

Fig. 10. Trade-off between production capacity and energy consumption: predicted Sherwood number as a function of Power number for the five spacer geometries and the results reported by [23].

3.1.4 Spacer Configuration Efficacy

As defined in Eq. (11), SCE is the ratio of Sherwood number to Power number, which represents both the mass transfer and energy consumption of SWMs. High SCE values are desirable for spacer configurations. As Fig. 11 shows, the Plain (empty channel) geometry has the maximum SCE due to its very low pressure drop, but it is an uncommon configuration to choose due to the absence of recirculation zones, which results in a high probability of deposit build-up on the membrane surface. Setting aside the Plain channel, the Ladder-type geometry has the highest SCE for low Reynolds numbers ($Re < 120$), while for $Re > 120$, the Wavy's SCE is slightly higher. The Triple geometry has the lowest SCE due to its high Pn.

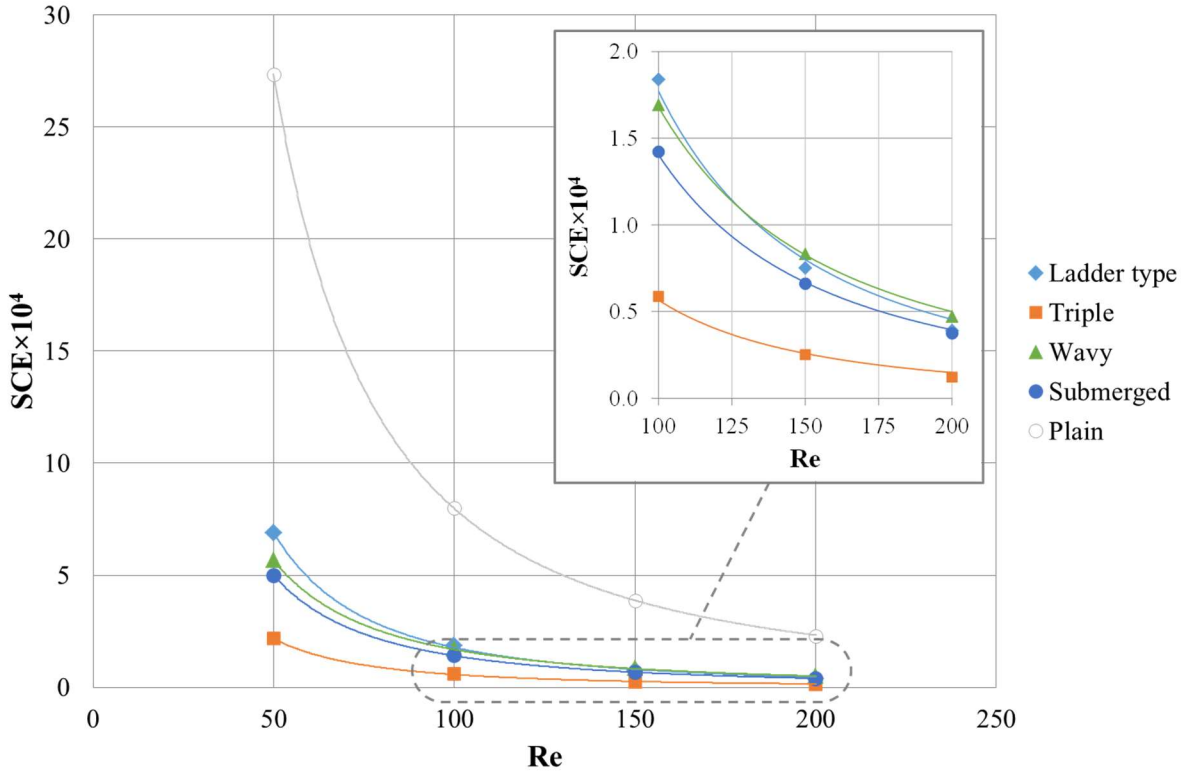

Fig. 11. Another perspective on the production capacity and energy consumption trade-off: predicted Spacer Configuration Efficacy as a function of Re.

3.2. Comparison of local velocities and concentrations

Figure 12 shows contour plots for the Wavy spacer configuration for fluid velocity (a and b) and salt concentration (c and d) at the outlet face (a and c) and on a longitudinal plane parallel to side walls positioned at z = 1 mm (b and d). The longitudinal plots show behaviour around the fifth unit cell (Fig. 4.), which is far enough from both inlet and outlet faces to be reflective of fully developed fluid flow [5] for Re = 50. Figure 13 shows the equivalent contour plots for Re = 200.

As evident from Fig. 12(b), the presence of the latitudinal filament creates a high velocity zone opposite the filament, decreasing the extent of the concentration polarization layer (Fig. 12d), which in turn enhances mass transfer. Fig. 12(b) shows the development of dead zones just before and just after the filament; the recirculating flow after the filament appears to help the solute to move away from the membrane wall into the bulk.

By increasing the flowrate fourfold, both high velocity and low velocity zones become more distinct elongated (Fig. 13b). As a result, the recirculating flows become more effective in moving solute away from the membrane (Fig. 13d). It should also be noted from Fig. 13(d) that the recirculating flow appears before the latitudinal filament moving the concentrated zone away from the membrane.

On the other hand, the outlet velocity contour plots (Figs 12a and 13a) show similar flow patterns for Re = 50 and 200, while the concentration contour plots (Figs 12c and 13c) reveal significant differences in the recirculating flows caused by the longitudinal filaments. For Re = 50, the recirculating flows spread over most of the channel width (Fig. 12c) whereas for Re = 200, they are

confined to the vicinity of the longitudinal filaments (Fig. 13c). It should be noted that Saeed [5] reported a similar pattern for longitudinal and latitudinal recirculating zones.

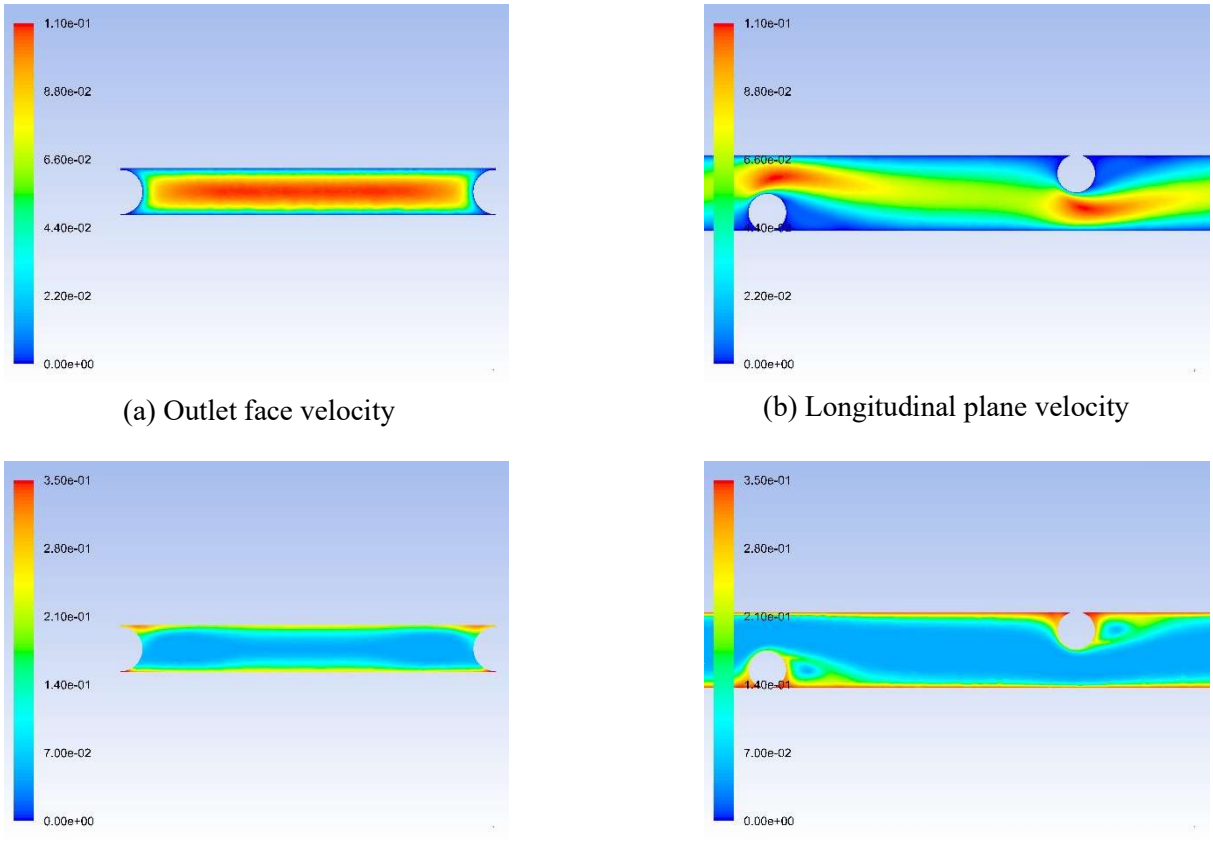

(a) Outlet face velocity

(b) Longitudinal plane velocity

(c) Outlet face concentration

(d) Longitudinal plane concentration

Fig. 12. Contour plots for the Wavy configuration for Re = 50.

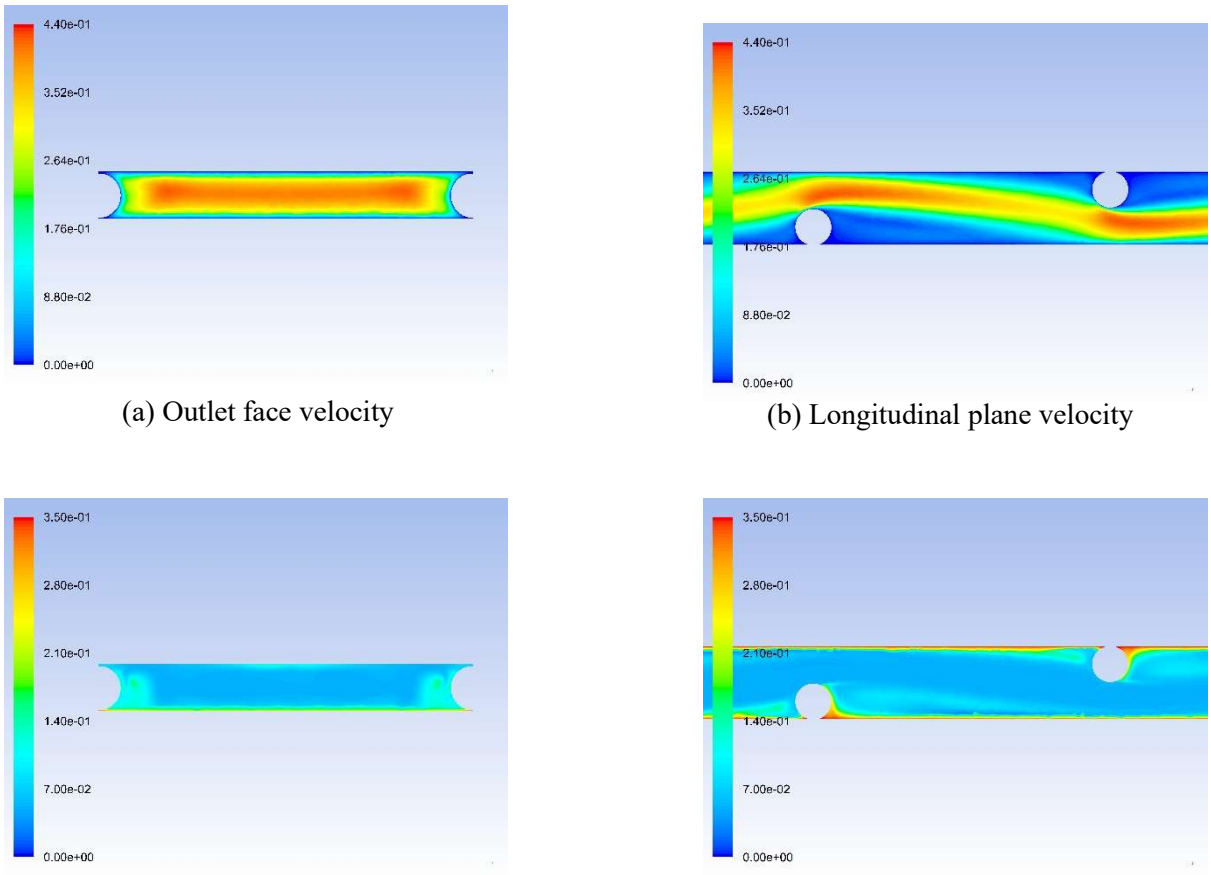

(a) Outlet face velocity

(b) Longitudinal plane velocity

(c) Outlet face concentration

(d) Longitudinal plane concentration

Fig. 13. Contour plots for the Wavy configuration for Re = 200.

3.3. Consistency of rankings obtained from alternative measures of spacer performance

Tables 5 and 6 report the rankings — from best performing to worst performing — of four of the feed spacers considered in this study based on five performance measures ($\Delta P/L$, SPC, Pn, Sh and SCE) and for low and high Reynolds numbers. The tables can be interpreted in three ways. Firstly, tracing along a row reveals the differences in ranking for a given feed spacer according to the different performance measures. Secondly, looking down a column shows the ranking of the spacers according to a given performance measure. Thirdly, comparing the same column in Tables 5 and 6 indicated the ranking's sensitivity to flowrate.

Table 5 shows that the common measures currently being used in the literature to assess spacer performance lead to different rankings for Re = 50 for the four feed spacer configurations studied. Even $\Delta P/L$, SPC and Pn, all of which focus on energy consumption, are not in agreement on the spacer ranking. On the other hand, comparing the data from Tables 5 and 6 reveals that the $\Delta P/L$ ranking varies with Reynolds number significantly, while SPC, Sh and SCE have one minor change – one swap between neighbours – and Pn has the same ranking for Re values of 50 and 200. Returning different results for different flowrates might be thought of as useful sensitivity or as unwelcome inconsistency. To the best of the authors' knowledge, this aspect is neither discussed nor addressed in previous studies in the literature including the merits and demerits of changes in ranking with flowrate.

The observed changes in spacer ranking (as reported in Tables 5 and 6), due to both the selection of the performance measure used and the changing flowrate, makes it critical to choose the performance measure carefully. Because the rankings it produced varied only a little with flowrate and it is the only measure considered that combines mass transfer and energy consumption, it is thought that the best performance measure to use of those considered here is SCE, as defined by Eq. (11) or with some modification. The authors found no previous study comparing different performance measures by relating them to more applied measures like the product unit cost, which might be the most interesting parameter for both membrane manufacturers and operators of membrane systems. Further investigations aimed at linking the various performance measures to capital and operating costs would prove to be more valuable in deciding which approach is most useful for assessing the performance of spacers.

Table 5
Comparison of spacer ranking using different performance measures at Re = 50. Key: **** indicates the most preferred spacer geometry (highest ranked), while * indicates the least preferred.

Configuration	$\Delta P/L$	SPC	Pn	Sh	SCE
Ladder	**	*	**	***	****
Triple	****	****	*	****	*
Wavy	***	**	***	**	***
Submerged	*	***	****	*	**
Min./max.	0.80	0.67	0.27	0.61	0.31

Table 6
Comparison of spacer ranking using different performance measures at Re = 200. Key: **** indicates the most preferred spacer geometry (highest ranked), while * indicates the least preferred.

Configuration	$\Delta P/L$	SPC	Pn	Sh	SCE
Ladder	*	*	**	**	***
Triple	**	***	*	****	*
Wavy	****	**	***	***	****
Submerged	***	****	****	*	**
Min./max.	0.82	0.71	0.19	0.57	0.26

3.4. Validation

In Table 7, the approach used in the present study is compared with some previous studies [6, 23, 29], which all use Ladder-type spacers, but of slightly different sizes as noted in the table. It is evident that the top and bottom shear stresses are 8% and 15% different from the average values reported by [6, 29], respectively. The lower pressure drop and dimensionless pressure drop observed in comparison with previous studies is thought to be acceptable given that the channel height is 23% larger in the present study. The Power number is proportional to $\Delta P \times H^4$ as shown in Eq. (7). The effect of 40% lower ΔP and 23% higher H will lead to a 17% difference in Pn results.

Table 7
Comparison of hydraulic results obtained using the approach developed in the present study with literature results for Re = 100 with a Ladder-type spacer.

Parameter	[29] [a]	[23] [b]	[6] [c]	Present study [d]
Average shear stress on top wall (N/m^2)	1	-	1.15	0.915
Average shear stress on bottom wall (N/m^2)	0.16	-	0.20	0.165
Pressure drop, $\Delta P/L$ (kPa/m)	5	-	6.29	3.859
Power number, $Pn \times 10^{-5}$	-	1.7	1.80	2.946
Dimensionless pressure drop, ΔP^*	-	-	0.32	0.192

a. Value interpolated from plot of filament spacing vs average shear stress on walls and linear pressure drop by [6].
b. Value reported for $L = 4d$.
c. Value reported for $L = 4.1d$ and $H = 0.772$ mm.
d. Value reported for $L = 4.1d$ and $H = 1$ mm.

Mass transfer results are compared with the previous study of Saeed, Vuthaluru and Vuthaluru [13] as shown in Table 8. Unlike the hydraulic behaviour, there is a significant difference between the current and previous results. As mentioned in their study [13], the concentration boundary condition on the membrane surface was assumed to be a salt mass fraction of 1. On the other hand, in the present study, the salt mass fraction on the membrane surface was assumed to be the saturation value, 0.35 w/w.

Furthermore, the Sherwood number is related to the mass transfer coefficient, which is inversely proportional to the salt concentration difference. As clarified earlier, the present study considers a boundary concentration much lower than used in previous studies. Thus, the lower concentration difference in the present study would result in lower mass transfer, but a higher mass transfer coefficient. Simulations show that reducing the concentration to one third will nearly double the mass transfer coefficient, leading to a nearly twofold increase in the Sherwood number and SCE (Table 8).

The above issue is significant because Sherwood number is commonly correlated as a function of Reynolds number, Schmidt number and geometry, which makes Sh independent of the solute concentration, assuming a negligible influence of concentration on physical properties. To the best of our knowledge, however, no published studies have investigated the change in Sh resulting from a constant surface concentration boundary condition compared to other types of boundary conditions at the membrane.

Another validation is done to ensure the current model produces a similar pattern of results to that established in previous work. The model was run in the Ladder-type geometry with the same boundary conditions as used by the previous study [13] and the results were found to be similar. The maximum difference is in the Power number, which was about 11% different from the previously reported value, while Sh and SCE are in closer agreement (Table 8). The different results observed might be due to several factors, including a different meshing method and accuracy in the vicinity of the cylinder-plane contact point, which has been addressed earlier in Section 2.5.

Table 8
Comparison of mass transfer results obtained using the approach developed in the present study with literature results for Re = 100 with a Ladder-type spacer.

Study and comparison details	Dimensionless spacer size [a]		Property			
	Channel length, L/H	Channel width, W/H	Average mass transfer coefficient, $k \times 10^5$ (m/s)	Sherwood number, Sh	Power number, Pn × 10^{-3}	Spacer Configuration Efficacy, SCE × 10^4
Saeed, Vuthaluru and Vuthaluru [13]	3.5	3.5	3.74	29	473.1	0.66
	3.5	4.5	3.75	31	329.7	0.94
	4.5	3.5	3.55	29	348.9	0.84
	4.5	4.5	3.64	31	259.1	1.21
Linearly interpolated from [13]	4.1	4.1	3.66	30	331.8	0.97
Current study	4.1	4.1	6.38	54.2	294.6	1.84
Current study with same boundary conditions as [13]	4.1	4.1	3.25	27.6	296.8	0.93
Difference between current study and linear interpolation of [13] for same boundary conditions	–	–	11.1%	8.5%	10.6%	4.0%

a. The study [13] used different definitions of channel size compared to the current study (Fig. 3). To facilitate comparison, the L/H and W/H values from [13] reported here have been adjusted to make them consistent with the current study.

As reported in Table 4, the present study has developed equations for Sh as a function of Re for various spacer geometries, which is similar to work conducted by In Seok and Ho Nam [15]. The present study reports values of 0.34 and 0.55 as the exponents of Re for Ladder-type and Wavy geometries, respectively, while [15] reports 0.294 and 0.475 for Cavity and Zigzag configurations, respectively, as shown in Table 1. In terms of configuration, Cavity and Ladder-type are similar, and Zigzag and Wavy are similar, with the main difference in both cases being the presence of longitudinal filaments in the Ladder-type and Wavy geometries. The introduction of longitudinal filaments leads to Re exponents that are about 20% higher in both cases. On the other hand, it should be noted that the highest exponent in the present study, 0.55 for the Wavy configuration, is smaller than the value of 0.875 reported by Schock and Miquel [16] for commercial spacers as seen in Table 1. The difference might be attributed to two main factors: better performance of the tested commercial spacer as well as lower inlet salinity, 0.03%, compared to 5% in the present work.

4. Conclusions

Computational fluid dynamics was used to study the effect of changing flowrate on four different feed spacer configurations, along with an empty channel, for spiral wound modules used in reverse

osmosis systems. Both flow and overall mass transfer phenomena were investigated by calculating various performance measures (such as Power number, Sherwood number and a relatively recent measure, the Spacer Configuration Efficacy) from the CFD results. Simulations were performed using the new saturated boundary condition. The results were validated against the previous literature.

The following conclusions are drawn from this study:

- The new saturated concentration boundary condition employed at the membrane surface resulted in nearly doubling of the predicted mass transfer coefficient compared to previous studies that used a pure solute boundary condition. This finding shows the importance feed-side membrane boundary conditions in RO simulations.
- Tetrahedral meshing of the fluid domain resulted in faster and more stable convergence than hexahedral meshing used in many previous studies.
- The performance measures were strongly affected by the Reynolds number of the flow in the range $50 \leq Re \leq 200$ and the spacer geometry.
- The simple power law correlations of the various performance measures with Re for each feed spacer that were developed allow rapid evaluation of spacer performance for planning purposes and facilitate comparison with other studies.
- Different performance measures lead to different rankings of the feed spacers and the ranking may change with Reynolds number. This situation is not entirely satisfactory and further work should be devoted to relating the current performance measures to more industrially-relevant measures, such as ones based on capital and operating costs.
- The SCE concept, which has been applied to feed spacer configurations other than Ladder-type to which it was previously restricted [5, 13], may be a good measure to use for selecting the best spacer configuration as it takes into account both flow and mass transfer performance, and did not vary as much with Re as pressure drop alone.
- According to SCE values for the four obstructed spacer geometries considered, the Ladder-type shows best results at Re values below 120, while Wavy is the best choice for Re values greater than 120; the benefits of using Wavy become greater with increasing Re.

Nomenclature

A_{eff}	Effective area (m^2)
A_i	Area of inlet face (m^2)
C_i	Inlet salt concentration (w/w)
C_m	Membrane salt concentration (w/w)
$\mathcal{D}$	Mass diffusivity (m^2/s)
d	Filament diameter (m)
D_h	Hydraulic diameter (m)
Eu	Euler number
H	Channel height (m)
k	Average mass transfer coefficient (m/s)
L	Channel length (m)

n Distance in direction normal to the filament (m)

P_0 Ambient pressure (Pa)

ΔP Pressure drop (Pa)

ΔP^* Dimensionless pressure drop

Pn Power number

Re_{ch} Channel Reynolds number

Re_{cyl} Cylinder Reynolds number

Re_h Hydraulic Reynolds number

SCE Spacer Configuration Efficacy

Sh Sherwood number

SPC Specific Power Consumption (W/m^3)

u_{eff} Effective velocity (m/s)

u Velocity in x direction (m/s)

$\dot{V}$ Volumetric flowrate (m^3/s)

v Velocity in y direction (m/s)

W Channel width (m)

w Velocity in z direction (m/s)

Greek symbols

α Flow angle of attack (°)

β Spacer geometry angle (°)

ϵ Porosity

μ Dynamic viscosity (Pa.s)

ρ Density (kg/m^3)

References

[1] J. Johnson, Engineering Aspects of Reverse Osmosis Module Design, Desalination and Water Treatment, 15 (2010) 236-248.
[2] Encyclopedia of Desalination and Water Resources: Energy Requirements of Desalination Processes, in, DESWARE.NET, http://www.desware.net/desa4.aspx, 2015.
[3] G. Belfort, Membrane modules: comparison of different configurations using fluid mechanics, Journal of Membrane Science, 35 (1988) 245-270.
[4] M. Shakaib, S.M.F. Hasani, I. Ahmed, R.M. Yunus, A CFD study on the effect of spacer orientation on temperature polarization in membrane distillation modules, Desalination, 284 (2012) 332-340.
[5] A. Saeed, Effect of feed channel spacer geometry on hydrodynamics and mass transport in membrane modules, PhD Thesis in Chemical Engineering, Curtin University, (2012).
[6] A. Saeed, R. Vuthaluru, Y. Yang, H.B. Vuthaluru, Effect of feed spacer arrangement on flow dynamics through spacer filled membranes, Desalination, 285 (2012) 163-169.
[7] Y.L. Li, P.J. Lin, K.L. Tung, CFD analysis of fluid flow through a spacer-filled disk-type membrane module, Desalination, 283 (2011) 140-147.
[8] S. Al-Sharif, M. Albeirutty, A. Cipollina, G. Micale, Modelling flow and heat transfer in spacer-filled membrane distillation channels using open source CFD code, Desalination, 311 (2013) 103-112.
[9] P. Sousa, A. Soares, E. Monteiro, A. Rouboa, A CFD study of the hydrodynamics in a desalination membrane filled with spacers, Desalination, 349 (2014) 22-30.
[10] M. Kostoglou, A.J. Karabelas, Comprehensive simulation of flat-sheet membrane element performance in steady state desalination, Desalination, 316 (2013) 91-102.
[11] Y.L. Li, K.L. Tung, Y.S. Chen, K.J. Hwang, CFD analysis of the initial stages of particle deposition in spiral-wound membrane modules, Desalination, 287 (2012) 200-208.
[12] A. Saeed, R. Vuthaluru, H. Vuthaluru, Concept of spacer configuration efficay (SCE) applied to optimize ladder type feed spacer filament spacing in narrow channels, in: International Conference On Water Desalination, Treatment and Management & Indian Desalination Association Annual Congress, Jaipur, India: The Malaviya National Institute of Technology., 2013.
[13] A. Saeed, R. Vuthaluru, H.B. Vuthaluru, Investigations into the effects of mass transport and flow dynamics of spacer filled membrane modules using CFD, Chemical Engineering Research and Design, 93 (2015) 79-99.
[14] A. Saeed, R. Vuthaluru, H.B. Vuthaluru, Impact of Feed Spacer Filament Spacing on Mass Transport and Fouling Propensities of RO Membrane Surfaces, Chemical Engineering Communications, 202 (2015) 634-646.
[15] K. In Seok, C. Ho Nam, The effect of turbulence promoters on mass transfer - numerical analysis and flow visualization, International Journal of Heat and Mass Transfer, 25 (1982) 1167-1181.
[16] G. Schock, A. Miquel, Mass-Transfer and Pressure Loss in Spiral Wound Modules, Desalination, 64 (1987) 339-352.
[17] A.R. Da Costa, A.G. Fane, D.E. Wiley, Spacer characterization and pressure drop modelling in spacer-filled channels for ultrafiltration, Journal of Membrane Science, 87 (1994) 79-98.
[18] S.K. Karode, A. Kumar, Flow visualization through spacer filled channels by computational fluid dynamics I. Pressure drop and shear rate calculations for flat sheet geometry, Journal of Membrane Science, 193 (2001) 69-84.
[19] Z. Cao, D.E. Wiley, A.G. Fane, CFD simulations of net-type turbulence promoters in a narrow channel, Journal of Membrane Science, 185 (2001) 157-176.
[20] J. Schwinge, D.E. Wiley, D.F. Fletcher, A CFD study of unsteady flow in narrow spacer-filled channels for spiral-wound membrane modules, Desalination, 146 (2002) 195-201.
[21] J. Schwinge, D.E. Wiley, D.F. Fletcher, Simulation of the flow around spacer filaments between narrow channel walls. 1. Hydrodynamics, Industrial & Engineering Chemistry Research, 41 (2002) 2977-2987.
[22] J. Schwinge, D.E. Wiley, D.F. Fletcher, Simulation of the flow around spacer filaments between channel walls. 2. Mass-transfer enhancement, Industrial & Engineering Chemistry Research, 41 (2002) 4879-4888.

[23] F. Li, W. Meindersma, A.B. de Haan, T. Reith, Experimental validation of CFD mass transfer simulations in flat channels with non-woven net spacers, Journal of Membrane Science, 232 (2004) 19-30.
[24] F. Li, W. Meindersma, A.B. de Haan, T. Reith, Optimization of commercial net spacers in spiral wound membrane modules, Journal of Membrane Science, 208 (2002) 289-302.
[25] F. Li, G.W. Meindersma, A.B. de Haan, T. Reith, Optimization of non-woven spacers by CFD and validation by experiments, Desalination, 146 (2002) 209-212.
[26] C.P. Koutsou, S.G. Yiantsios, A.J. Karabelas, Numerical simulation of the flow in a plane-channel containing a periodic array of cylindrical turbulence promoters, Journal of Membrane Science, 231 (2004) 81-90.
[27] V.V. Ranade, A. Kumar, Fluid dynamics of spacer filled rectangular and curvilinear channels, Journal of Membrane Science, 271 (2006) 1-15.
[28] J.L.C. Santos, V. Geraldes, S. Velizarov, J.G. Crespo, Investigation of flow patterns and mass transfer in membrane module channels filled with flow-aligned spacers using computational fluid dynamics (CFD), Journal of Membrane Science, 305 (2007) 103-117.
[29] M. Shakaib, S.M.F. Hasani, M. Mahmood, Study on the effects of spacer geometry in membrane feed channels using three-dimensional computational flow modeling, Journal of Membrane Science, 297 (2007) 74-89.
[30] G.A. Fimbres-Weihs, D.E. Wiley, Numerical study of mass transfer in three-dimensional spacer-filled narrow channels with steady flow, Journal of Membrane Science, 306 (2007) 228-243.
[31] Y.L. Li, K.L. Tung, CFD simulation of fluid flow through spacer-filled membrane module: selecting suitable cell types for periodic boundary conditions, Desalination, 233 (2008) 351-358.
[32] A. Cipollina, G. Micale, L. Rizzuti, Membrane distillation heat transfer enhancement by CFD analysis of internal module geometry, Desalination and Water Treatment, 25 (2011) 195-209.
[33] A. Cipollina, A. Di Miceli, J. Koschikowski, G. Micale, L. Rizzuti, CFD simulation of a membrane distillation module channel, Desalination and Water Treatment, 6 (2009) 177-183.
[34] M. Qureshi, M. Shakaib, CFD study for temperature and concentration profiles in membrane channels, in: International conference on Energy and Sustainability, NED University of Engineering & Technology, Karachi, Pakistan, 2013.
[35] C.P. Koutsou, S.G. Yiantsios, A.J. Karabelas, Direct numerical simulation of flow in spacer-filled channels: Effect of spacer geometrical characteristics, Journal of Membrane Science, 291 (2007) 53-69.
[36] S.M. Mojab, A. Pollard, J.G. Pharoah, S.B. Beale, E.S. Hanff, Unsteady Laminar to Turbulent Flow in a Spacer-Filled Channel, Flow, Turbulence and Combustion, 92 (2014) 563-577.
[37] V.A. Haaksman, A. Siddiqui, C. Schellenberg, J. Kidwell, J.S. Vrouwenvelder, C. Picioreanu, Characterization of feed channel spacer performance using geometries obtained by X-ray computed tomography, Journal of Membrane Science, 522 (2017) 124-139.
[38] M. Isaacson, A.A. Sonin, Sherwood number and friction factor correlations for electrodialysis systems, with application to process optimization, Industrial & Engineering Chemistry Process Design and Development, 15 (1976) 313-321.
[39] K.K. Lau, M.Z. Abu Bakar, A.L. Ahmad, T. Murugesan, Feed spacer mesh angle: 3D modeling, simulation and optimization based on unsteady hydrodynamic in spiral wound membrane channel, Journal of Membrane Science, 343 (2009) 16-33.
[40] A. Storck, D. Hutin, Energetic Aspects of Turbulence Promotion Applied to Electrolysis Processes, Canadian Journal of Chemical Engineering, 58 (1980) 92-102.
[41] A.J. Karabelas, M. Kostoglou, C.P. Koutsou, Modeling of spiral wound membrane desalination modules and plants - review and research priorities, Desalination, 356 (2015) 165-186.
[42] Y.L. Li, K.L. Tung, The effect of curvature of a spacer-filled channel on fluid flow in spiral-wound membrane modules, Journal of Membrane Science, 319 (2008) 286-297.
[43] M. Capobianchi, T.F. Irvine, N.K. Tutu, G.A. Greene, A new technique for measuring the Fickian diffusion coefficient in binary liquid solutions, Experimental Thermal and Fluid Science, 18 (1998) 33-47.
[44] J. Burgess, Metal ions in solution, Ellis Horwood, Chichester, 1978.
[45] CRC handbook of chemistry and physics (Online), 91st ed., CRC Press LLC, Boca Raton, FL, 2010.

[46] R.A. Serway, Physics for scientists & engineers, 3rd ed., Saunders College Pub., Philadelphia, 1992.